STUDY ON EM SCATTERING FROM 2-D TARGET ABOVE 1-D LARGE SCALE ROUGH SURFACE WITH LOW GRAZING INCIDENCE BY PARALLEL MOM BASED ON PC CLUSTERS

L.-X. Guo, A.-Q. Wang, and J. Ma

School of Science
Xidian University
No. 2 Taibai Road, Xi'an, Shaanxi, China

Abstract—Based on message passing interface (MPI) of the PC Clusters, the parallel method of moment (MOM) is applied to the electromagnetic (EM) scattering from one dimensional (1-D) large scale PEC Gaussian rough surface with two dimensional (2-D) PEC cylinder above it with low grazing incidence. The conjugate gradient method (CGM) for solving MOM matrix equation is parallelized according to the property of MPI in this work. The parallel computational efficiency and validity are shown by several numerical simulations, in which it is proved that the proposed method supplies a novel technique for solving the problem of the composite EM scattering for a 2-D target above 1-D large scale rough surface. Finally, the influences of root mean square (rms) height, the correlation length of the Gaussian surface, the size and the altitude of the cylinder, the polarization on the bistatic scattering coefficient (BSC) for low grazing incidence are also discussed in detail.

1. INTRODUCTION

Over the past decades, several researchers have been investigated the electromagnetic scattering from a rough surface with/without a target above it, and explored the electromagnetic scattering to the area of low-attitude/long-range radar surveillance, target tracking, navigation systems operation, and communication at low grazing conditions above the sea surface [1–8]. Many kinds of method, including analytical methods and numerical approach, have been used to calculate the

---

Corresponding author: L.-X. Guo (lxguo@mail.xidian.edu.cn).

electromagnetic scattering of this composite model. Due to the rigid limitations and low precisions, the methods based on the approximate analytical method [7, 9] is too weak to solve the composite scattering problem of large scale rough surface at low grazing incident angle. In order to solve this scattering problem, the simulated length of rough surface by Monte-Carlo method must be as long as possible, leading to large numbers of unknown. Dealing with such large unknowns, the computational time and memory requirements limit us using the method of moment (MOM) [10] to calculate this problem. Such numerical methods as the Generalized Forward-Backward Method (GFBM) [11], the generalized forward-backward method/spectrum acceleration algorithm (GFBM/SAA) [12], the banded-matrix-iterative-method/canonical-grid method (CAG) [13, 14] and the physics-based two-grid/canonical-grid method (PBTG/CAG) [15] have been applied widely to solve the EM scattering from 1-D large scale rough surface with or without a 2-D target above it by Monte-Carlo simulations. The time-domain and frequency-domain scattering characteristics of 3-D penetrable object above a 2-D lossy dielectric rough interface are studied in [16] by using an iterative MOM solution for equivalent electric and magnetic surface current densities on the rough interface and equivalent volumetric electric current in the penetrable object. Different from these fast numerical algorithms, in this paper the parallel MOM is applied to solve the scattering problem of a target above a large scale rough surface at low grazing incident angle.

Low cost of the parallel computing platform based on the PC Clusters makes its application for calculating EM scattering becomes more and more popular. In order to solve large scale linear equation generated by MOM for 1-D rough surface scattering at low grazing incident angle, the parallelized conjugate gradient method (CGM) [17] is investigated base on the property of the message passing interface (MPI) of the PC Clusters system in our work. From the numerical simulations, it is found significantly that the parallel MOM supplies a novel technique for solving 1-D large scale rough surface scattering with low grazing incidence. Finally, the influences of rough surface parameters and polarization on the bistatic scattering coefficient (BSC) at low grazing incident angle are discussed in detail.

2. DESCRIPTION OF THE PROBLEM

Consider an incident electromagnetic wave impinging upon a PEC cylinder with radius r and is located a distance h above a 1-D PEC random rough surface with height profile function $z = f(x)$ as shown
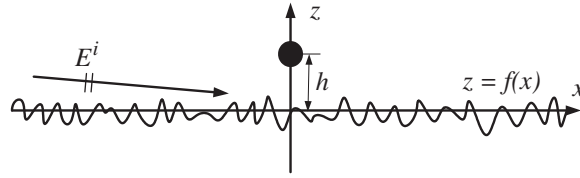
Figure 1. Geometry for EM scattering from the target above the rough surface with low grazing incidence.

in Fig. 1, where $f(x)$ is a Gaussian distributed rough surface, with correlation length l and root mean square height (rms) σ [18]. In this paper, the time dependence is $e^{-i\omega t}$ and the 2-D position vector is $\mathbf{r} = x\hat{\mathbf{x}} + z\hat{\mathbf{z}}$.

For horizontal polarized (HH) incidence, the incident electric field can be written as

$$\mathbf{E}^i(\mathbf{r}) = \varphi_e^i(\mathbf{r})\hat{\mathbf{y}} \tag{1}$$

If the total electric field of the free space is $\mathbf{E}^t(\mathbf{r}) = \varphi_e^t(\mathbf{r})\hat{\mathbf{y}}$, we can obtain the electric field integral equation (EFIE) [19] for a 2-D PEC target above 1-D PEC rough surface scattering under horizontal polarized incidence as following

$$\varphi_e^i(\mathbf{r}) = \int_{S_s} ds' g(\mathbf{r}, \mathbf{r}')\hat{\mathbf{n}}' \cdot \nabla' \varphi_e^t(\mathbf{r}') + \int_{S_t} ds' g(\mathbf{r}, \mathbf{r}')\hat{\mathbf{n}}' \cdot \nabla' \varphi_e^t(\mathbf{r}') \tag{2}$$

where $g(\mathbf{r}, \mathbf{r}')$ is the two dimensional Green's function, $g(\mathbf{r}, \mathbf{r}') = \frac{i}{4} H_0^{(1)}(k_0 |\mathbf{r} - \mathbf{r}'|)$, k_0 is the wave number of the free space and $H_0^{(1)}(\cdot)$ is the zeroth-order Hankel function of the first kind, S_s, S_t denote the rough surface and the target boundary, respectively, and $\hat{\mathbf{n}}$ is unit normal vector on them. Using MOM, the above EFIE can be discretized into matrix equation

$$\overline{\overline{A}} \cdot \bar{U} = \bar{b} \tag{3}$$

where the matrix elements as

$$\overline{\overline{A}} = \begin{bmatrix} \overline{\overline{A}}_{ss} & \overline{\overline{A}}_{st} \\ \overline{\overline{A}}_{ts} & \overline{\overline{A}}_{tt} \end{bmatrix}, \quad \bar{U} = \begin{bmatrix} \bar{U}_s \\ \bar{U}_t \end{bmatrix}, \quad \bar{b} = \begin{bmatrix} \bar{b}_s \\ \bar{b}_t \end{bmatrix} \tag{4}$$

where the subscript s and t represent the rough surface and the target boundary, separately. And the elements of the impedance matrix $\overline{\overline{A}}$ in

detail

$$
A_{mn} = \begin{cases} \dfrac{i}{4}\Delta l_n H_0^{(1)}\left(k_0\left|\mathbf{r}_m - \mathbf{r}_n\right|\right) & m \neq n \\[2mm] \dfrac{i}{4}\Delta l_n\left(1+\dfrac{i2}{\pi}\ln\left(\dfrac{\gamma k_0 \Delta l_m}{4e}\right)\right) & m = n \end{cases} \quad , \quad m,n \in S_s \text{ or } S_t \quad (5a)
$$

$$
b_m = \varphi_e^i\left(x_m, f\left(x_m\right)\right), \quad m \in S_s \text{ or } S_t \tag{5b}
$$

where the subscript m and n is from the field point and source point, respectively. For vertical polarization (VV), the magnetic field of the incident wave can be proposed as

$$
\mathbf{H}^i(\mathbf{r}) = \varphi_m^i(\mathbf{r})\hat{\mathbf{y}} \tag{6}
$$

and when the total magnetic field of the free space is $\mathbf{H}^t(\mathbf{r}) = \varphi_m^t(\mathbf{r})\hat{\mathbf{y}}$, we can obtain the magnetic field integral equation (MFIE) [19] for 2-D PEC target over a 1-D PEC rough surface scattering under vertical polarized incidence as following

$$
\varphi_m^i(\mathbf{r}) + \int_{\mathrm{PVS}_s} ds' \varphi_m^t(\mathbf{r}')\hat{\mathbf{n}}' \cdot \nabla' g(\mathbf{r},\mathbf{r}')
$$

$$
+ \int_{\mathrm{PVS}_t} ds' \varphi_m^t(\mathbf{r}')\hat{\mathbf{n}}' \cdot \nabla' g(\mathbf{r},\mathbf{r}') = \frac{1}{2}\varphi_m^t(\mathbf{r}) \tag{7}
$$

where, $\int_{\mathrm{PVS}_s}$, $\int_{\mathrm{PVS}_t}$ refer to the Cauchy principal value integral on the rough surface and the target boundary, respectively. Same as the horizontal case, the matrix equation for vertical incidence can be also obtained by MOM

$$
\overline{\overline{B}} \cdot \bar{V} = \bar{I} \tag{8}
$$

Due to the space limitation, the concrete elements of this matrix are not shown here. To avoid the artificial edge diffraction resulting from finite length of the simulated rough surface, the incident wave can not be simply chosen as a plane wave, and should be expressed as a tapered wave in which the energy is distributed in a narrow beam about the mean incident angle. In this study, we choose the tapered wave suggested by Thorsos [18] which satisfies the requirement and the Maxwell's equation in an appropriate sense. Consider a tapered incident plane wave illuminate the geometry shown in Fig. 1, and the incident tapered plane wave can be expressed as

$$
\varphi^i(\mathbf{r}) = \exp(ik_0(x\sin\theta_i - f(x)\cos\theta_i)(1+w(\mathbf{r})))\exp\left(-\frac{(x+f(x)\tan\theta_i)^2}{g^2}\right) \tag{9}
$$

where $w(\mathbf{r}) = [2(x + f(x)\tan\theta_i)^2/g^2 - 1]/(k_0 g\cos\theta_i)^2$, θ_i is the incident angle defined with respect to the normal in the counterclockwise direction, g is the tapering parameter with dimension of the length and controls the tapering of incident wave. Typically, the MOM is applied to a domain of the rough surface length is L. As the basis of the tapered incident wave, the tapering parameter g and L at least should satisfy all requirements of the wave equation, correlation length, and energy truncation, which results in [20]

$$g > \frac{6}{(\cos\theta_i)^{1.5}} \tag{10}$$

$$L > 15l \text{ and } L \geq 4g \tag{11}$$

From Equation (10) and Equation (11), it can be easily observed that, for low grazing incident angle, the length of simulated rough surface L must be long enough in order to make numerical simulations effective. In Fig. 2, we plot the distribution of the magnitude of the incident wave $\left|\varphi^i\right|$ at low grazing incident angle $\theta_i = 85°$, with $L = 1500\lambda$ and $g = L/6$. Although, the incident angle is very large, the distribution of $\left|\varphi^i\right|$ still avoid the artificial edge reflection thanks to the large scale length of the simulated rough surface, which guarantees the accuracy of the numerical experiments in this work.
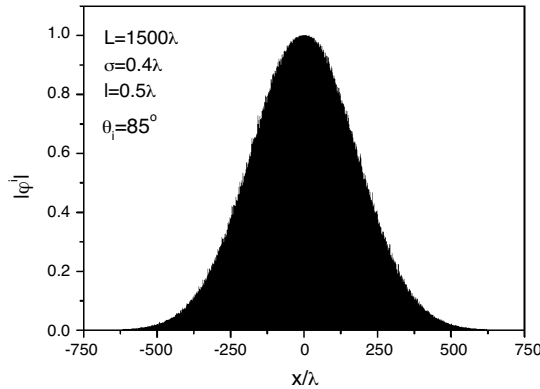
Figure 2. The magnitude of the incident field (electric and magnetic) with low grazing incidence.

3. CONJUGATE GRADIENT METHOD AND ITS PARALLELIZATION

In the past few years, the computational power of commodity PCs has been doubling about every eighteen months. At the same time, network interconnects that provide very low latency and very high band-width are also emerging. This trend makes it promising to build high performance computing by clustering, which combines the computational power of commodity PCs and the communication performance of high speed network interconnects.

In this work, the parallel numerical simulations are experimented through PC Clusters. A typical parallel computing PC cluster system are composed of several PCs and a high speed interconnect which are used to establish a small-scale local area network as presented in Fig. 3.
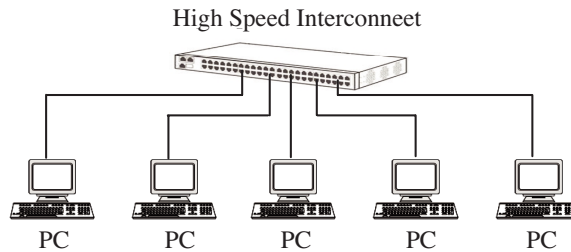
Figure 3. The composition of PC clusters.

There are many prominent advantages to conduct parallel computing on PC Clusters, for example smaller investment, easier programming, more flexible architecture, higher cost-effective, more scalability comparing to the expensive supercomputers and appropriative parallel computer systems.

The main Clusters configuration in this research is as follows

1) System composing: 8 PCs;
2) For each PC CPU: Intel Pentium 4, 2.4 GHz;

> Memory : 1 GB;
> Main-board: ASUS P5KSE;

3) Switch: TP-Link TL-R402M 1000M;
4) Operation: Windows XP;
5) Programming environment: MPICH2Visual Fortran.

MPI (Message Passing Interface) [21, 22] is a language-independent communications protocol used to program parallel computers, in which both point-to-point and collective communication are supported. MPI's goals are high performance, scalability, and portability and it remains the dominant model used in high-performance computing today. Because MPI is not sanctioned by any major standards body; nevertheless, it has become a de facto standard for communication among processes that model a parallel program running on a distributed memory system. Actual distributed memory supercomputers such as computer clusters often run these programs. Based on the above advantages, we adopt MPICH 2.103 to construct MPI platform on the PC Clusters in this research.

In this paper, the CGM is parallelized to solve matrix equation according to the property of MPI, in which the impedance matrix is divided by lines for different processes involved in the parallel computing system. For a general nonsingular complex matrix equation as below

$$\overline{\overline{A}} \cdot \bar{x} = \bar{b} \tag{12}$$

We use CGM to solve the equation as procedure given in Fig. 4, $\langle \cdot \rangle$ and $\|\cdot\|$ stand for the inner space product and the norm number, respectively. For two vectors $\bar{x} = [x_1, x_2, \ldots, x_n]^{\mathrm{T}}$, $\bar{y} = [y_1, y_2, \ldots, y_n]^{\mathrm{T}}$, $\langle \bar{x}, \bar{y} \rangle = \sum_{i=1}^{n} x_i y_i^*$, $\|\bar{x}\| = \sqrt{\langle \bar{x}, \bar{x} \rangle} = \sqrt{\sum_{i=1}^{n} |x_i|^2}$, superscript "*" and "+" denote conjugate and associate respectively. ε is the residual, and here we choose $\varepsilon = 0.001$.

With the purpose of making each process involved in the paralleling computing system has a balanceable task, the whole impedance matrix must be divided averagely. If the impedance matrix is divided in chessboard, the number of the processes must be $N \times N$ ($N = 2, 3, 4, \ldots$) which will be limited by the hardware of the parallel system. To overcome this shortcoming, the matrix should be divided by lines or rows. In the CGM, the product $\overline{\overline{A}} \cdot \bar{x}$ of the matrix $\overline{\overline{A}}$ and a vector $\bar{x}$, the product $\overline{\overline{A}}^{+} \cdot \bar{x}$ of the matrix $\overline{\overline{A}}^{+}$ and a vector $\bar{x}$ must be computed, which is a critical step to realize the two products on the parallel system, where $\overline{\overline{A}}^{+}$ is the associated matrix of $\overline{\overline{A}}$. Here, we take 8×8 matrix shown in Fig. 5(a) and Fig. 5(b) as an example. The first subscript of the matrix's and vector's elements denotes the number of the processes where the elements are stored.

The product of the matrix and the vector:

Process 0: $\sum_{i=1}^{8} a_{0i} \times x_{0i} = b_0$
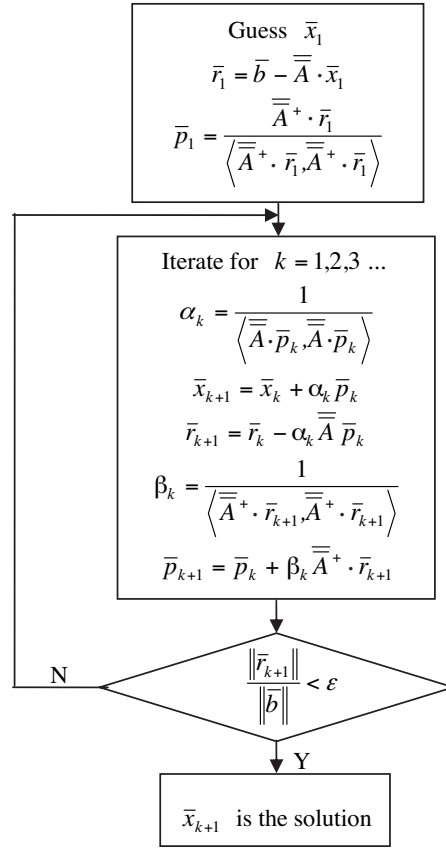
Figure 4. The procedure of the conjugate gradient method.

Process j: $\sum_{i=1}^{8} a_{ji} \times x_{ji} = b_j$ $(j = 1, \dots, 7)$, then send b_j to Process 0, the final product $\bar{y} = [b_0 \ b_1 \ b_2 \ b_3 \ b_4 \ b_5 \ b_6 \ b_7]^{\mathrm{T}}$

The product of the associated matrix and the vector:

Process 0: $b_{0i} = a_{0i}^* x_{01}$ $(i = 1, \dots, 8)$ obtain vector $[b_{01} \ b_{02} \ b_{03} \ b_{04} \ b_{05} \ b_{06} \ b_{07} \ b_{08}]^{\mathrm{T}}$

Process j: $b_{ji} = a_{ji}^* x_{j(j+1)}$ $(i = 1, \dots, 8)$ obtain vector $[b_{j1} \ b_{j2} \ b_{j3} \ b_{j4} \ b_{j5} \ b_{j6} \ b_{j7} \ b_{j8}]^{\mathrm{T}}$ $(j = 1, \dots, 7)$, then send the vector to Process 0, the final product $\bar{y} = [y_1 \ y_2 \ y_3 \ y_4 \ y_5 \ y_6 \ y_7 \ y_8]^{\mathrm{T}}$ where $y_m = \sum_{k=0}^{7} b_{km}$, $(m = 1, \dots, 8)$.

$$\begin{bmatrix} a_{01} & a_{02} & a_{03} & a_{04} & a_{05} & a_{06} & a_{07} & a_{08} \\ a_{11} & a_{12} & a_{13} & a_{14} & a_{15} & a_{16} & a_{17} & a_{18} \\ a_{21} & a_{22} & a_{23} & a_{24} & a_{25} & a_{26} & a_{27} & a_{28} \\ a_{31} & a_{32} & a_{33} & a_{34} & a_{35} & a_{36} & a_{37} & a_{38} \\ a_{41} & a_{42} & a_{43} & a_{44} & a_{45} & a_{46} & a_{47} & a_{48} \\ a_{51} & a_{52} & a_{53} & a_{54} & a_{55} & a_{56} & a_{57} & a_{58} \\ a_{61} & a_{62} & a_{63} & a_{64} & a_{65} & a_{66} & a_{67} & a_{68} \\ a_{71} & a_{72} & a_{73} & a_{74} & a_{75} & a_{76} & a_{77} & a_{78} \end{bmatrix} \begin{bmatrix} x_{(0-7)1} \\ x_{(0-7)2} \\ x_{(0-7)3} \\ x_{(0-7)4} \\ x_{(0-7)5} \\ x_{(0-7)6} \\ x_{(0-7)7} \\ x_{(0-7)8} \end{bmatrix} \quad \begin{bmatrix} a_{01}^* & a_{11}^* & a_{21}^* & a_{31}^* & a_{41}^* & a_{51}^* & a_{61}^* & a_{71}^* \\ a_{02}^* & a_{12}^* & a_{22}^* & a_{32}^* & a_{42}^* & a_{52}^* & a_{62}^* & a_{72}^* \\ a_{03}^* & a_{13}^* & a_{23}^* & a_{33}^* & a_{43}^* & a_{53}^* & a_{63}^* & a_{73}^* \\ a_{04}^* & a_{14}^* & a_{24}^* & a_{34}^* & a_{44}^* & a_{54}^* & a_{64}^* & a_{74}^* \\ a_{05}^* & a_{15}^* & a_{25}^* & a_{35}^* & a_{45}^* & a_{55}^* & a_{65}^* & a_{75}^* \\ a_{06}^* & a_{16}^* & a_{26}^* & a_{36}^* & a_{46}^* & a_{56}^* & a_{66}^* & a_{76}^* \\ a_{07}^* & a_{17}^* & a_{27}^* & a_{37}^* & a_{47}^* & a_{57}^* & a_{67}^* & a_{77}^* \\ a_{08}^* & a_{18}^* & a_{28}^* & a_{38}^* & a_{48}^* & a_{58}^* & a_{68}^* & a_{78}^* \end{bmatrix} \begin{bmatrix} x_{01} \\ x_{12} \\ x_{23} \\ x_{34} \\ x_{45} \\ x_{56} \\ x_{67} \\ x_{78} \end{bmatrix}$$

(a)   (b)

Figure 5. (a) The product of the matrix and the vector. (b) The product of the associated matrix and the vector.

4. NUMERICAL RESULTS AND DISCUSSIONS

After solving the matrix equation like Equation (3) and Equation (8), we can get the scattered electric field and the scattered magnetic field of the composite model for horizontal and vertical cases, respectively.

$$\varphi^s \left(\mathbf{r}' \right) = \frac{i}{4} \sqrt{\frac{2}{\pi k_0 r'}} e^{-i\frac{\pi}{4}} e^{ik_0 r'} \varphi_s^{(N)} \left(\theta_s \right) \tag{13}$$

where, for HH polarized incidence, we have

$$\varphi_s^{(N)} \left(\theta_s \right) = \int_{S_s} ds U \left(\mathbf{r} \right) e^{-ik_0 (x \sin \theta_s + f(x) \cos \theta_s)}$$

$$+ \int_{S_t} ds U \left(\mathbf{r} \right) e^{-ik_0 (x \sin \theta_s + q(x) \cos \theta_s)} \tag{14a}$$

and for VV polarization,

$$\varphi_s^{(N)} \left(\theta_s \right) = - \int_{S_s} ds V \left(\mathbf{r} \right) ik_0 \left(\hat{\mathbf{n}} \cdot \hat{\mathbf{R}} \right) e^{-ik_0 (x \sin \theta_s + f(x) \cos \theta_s)}$$

$$+ \int_{S_t} ds V \left(\mathbf{r} \right) ik_0 \left(\hat{\mathbf{n}} \cdot \hat{\mathbf{R}} \right) e^{-ik_0 (x \sin \theta_s + q(x) \cos \theta_s)} \tag{14b}$$

where $q(x)$ is the height profile function of target, $\hat{\mathbf{R}} = \sin \theta_s \hat{\mathbf{x}} + \cos \theta_s \hat{\mathbf{z}}$ is the unit vector of far region. Then we have the BSC as
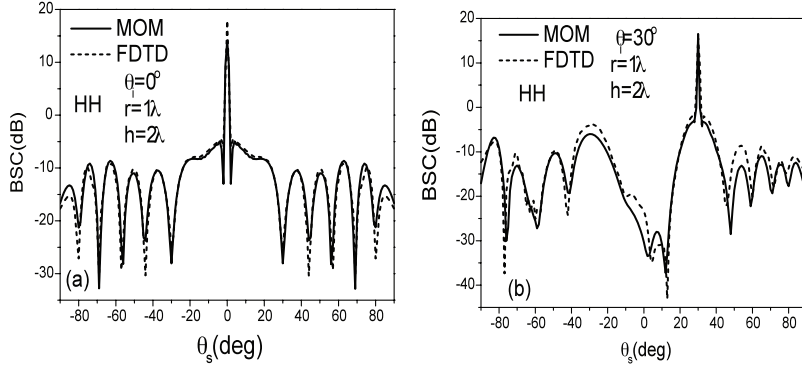
Figure 6. The comparison of parallel MOM and FDTD for a PEC cylinder above a flat surface.

$$\text{BSC}\,(\theta_s) = \frac{\left|\varphi_s^{(N)}\,(\theta_s)\right|^2}{8\pi k_0 g \sqrt{\dfrac{\pi}{2}}\cos\theta_i\left[1 + \dfrac{1 + 2\tan^2\theta_i}{2k_0^2 g^2 \cos^2\theta_i}\right]} \tag{15}$$

In order to examine the validity of the scattering formulation, we first compute the BSC of a PEC cylinder above a flat PEC surface, and the numerical results are presented by MOM and FDTD in Fig. 6. It is obvious that the two methods are in fairly good agreement, which indicates the validity of MOM for composite scattering. It should be pointed out that the numerical results of BSC for a PEC cylinder above a PEC rough surface by MOM have been compared and verified with those by FDTD in our previous published paper [3].

The comparison of calculating time and acceleration ratio for one surface realization with $\sigma = 0.1\lambda$, $l = 0.3\lambda$, $L = 409.6\lambda$, $\theta_i = 30°$, with a cylinder of which the radius $r = 5\lambda$, the height $h = 10\lambda$, 10 sampling points per λ experimented by different number of the processes are illustrated in Fig. 7. Let t_p denotes the time that one simulation cost by p processes, where $p = 1, 2, 4, 6, 8$, the acceleration ratio S_p is defined as following

$$S_p = \frac{t_1}{t_p} \tag{16}$$

The computing time consumed by the parallel MOM is mainly made up of two parts, the filling time of the impedance matrix and the solving time of the matrix equation by the parallelized CGM. In order to reduce the communication time between the processes,

the data of the rough surface are stored in every process, so the communication is totally used by the parallelized CGM. In Fig. 7, the total time are composed of the generating time of the matrix elements and the solving time of the matrix equation by the parallel CGM. It can be found that the parallel acceleration ratio is almost in direct proportion to the numbers of processes involved in the computing parallel system, the acceleration ratio increases linearly with processes growing in number. Although this acceleration ratio is obtained under the small incidence simulation, for the low grazing incidence, it will present same characteristic due to the feature of the parallel MOM, which indicates that 1-D large scale rough EM scattering problem can be solved by this proposed technique.
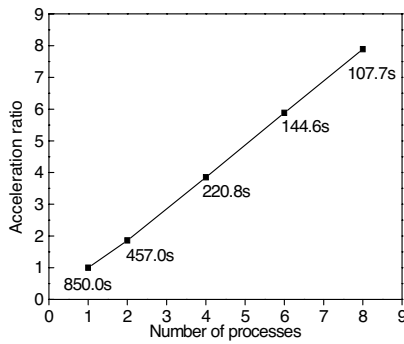
Figure 7. The simulating time and acceleration ratio.
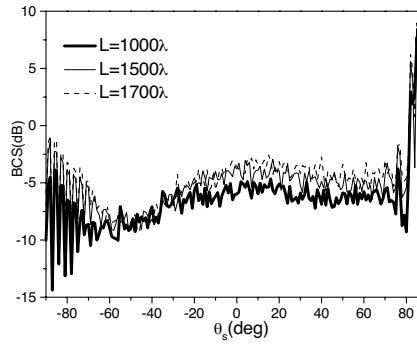
Figure 8. Comparison of BSC for different surface length.

Figure 8 depicts the BSC from a cylinder with $r = 5\lambda$, $h = 10\lambda$ above the simulated rough surface with different length L for HH polarization, and a Gaussian rough surface is given with $\sigma = 0.5\lambda$, $l = 1.0\lambda$ for the tapered wave incidence with $g = L/6$ at low grazing incident angle $\theta_i = 85°$. It is observed that, the results of $L = 1500\lambda$ and $L = 1700\lambda$ overlap each other which validates the choosing rule of g and L in Equation (10) and Equation (11), and guarantees the stability of the below numerical simulations. It should be noted that all the following numerical results are complemented with the simulated length $L = 1500\lambda$, 10 sampling points per wavelength λ, 100 surfaces realizations and 8 processes.

In order to compare the different scattering characteristics between the small incidence $\theta_i = 30°$ and low grazing incidence $\theta_i = 85°$, the BSC of these two incident cases are calculated by MOM and plotted in Fig. 9. In performing the calculation, the cylinder target with $r = 20\lambda$, $h = 25\lambda$ above the surface are given, where surface
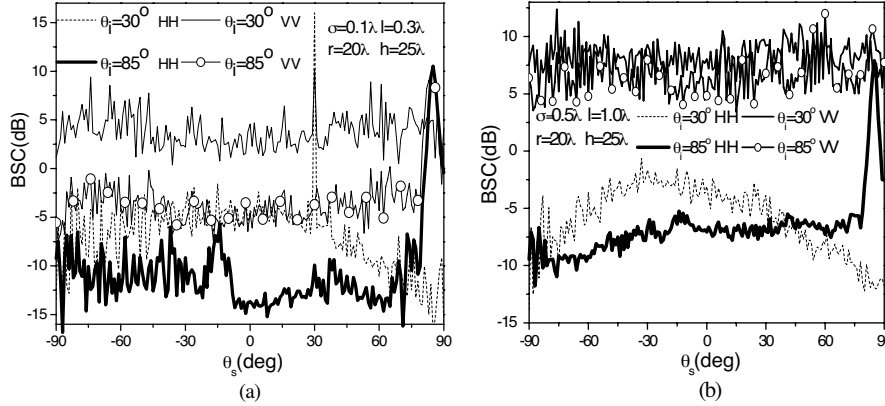
Figure 9. Distribution of BSC for different surface parameters, incident angle and polarization.
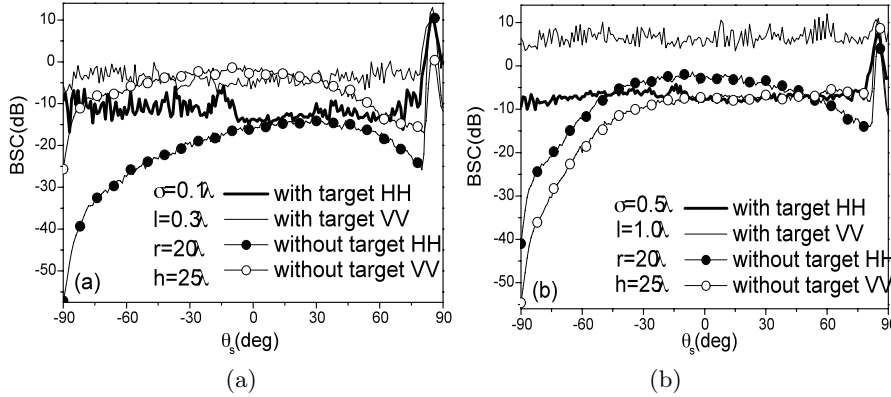
Figure 10. Distribution of BSC from Gaussian surface with/without PEC target.

parameter $\sigma = 0.1\lambda$, $l = 0.3\lambda$ and $\sigma = 0.5\lambda$, $l = 1.0\lambda$ corresponding to Fig. 9(a) and Fig. 9(b), respectively. It is shown that the BSC of HH is evidently smaller than that of VV over almost all scattering region. In Fig. 9(a), due to the smaller roughness, there is an obvious peak in the specular direction for both $\theta_i = 30°$ and $\theta_i = 85°$, especially for HH polarization. In Fig. 9(b), it can be easily observed that, due to the larger roughness, there isn't any peak in the whole scattering angle for small incident angle, whereas there is a big peak appearing in the specular direction for the low grazing incident angle.

To further explore the important scattering characteristic of BSC
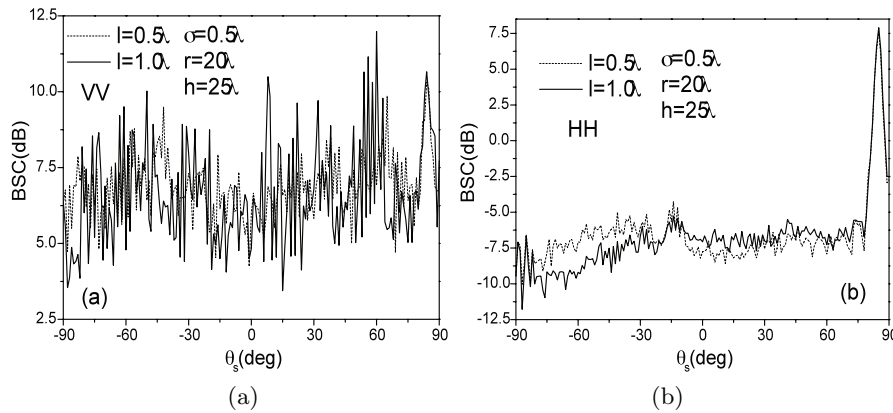
Figure 11. BSC for different l and polarization.
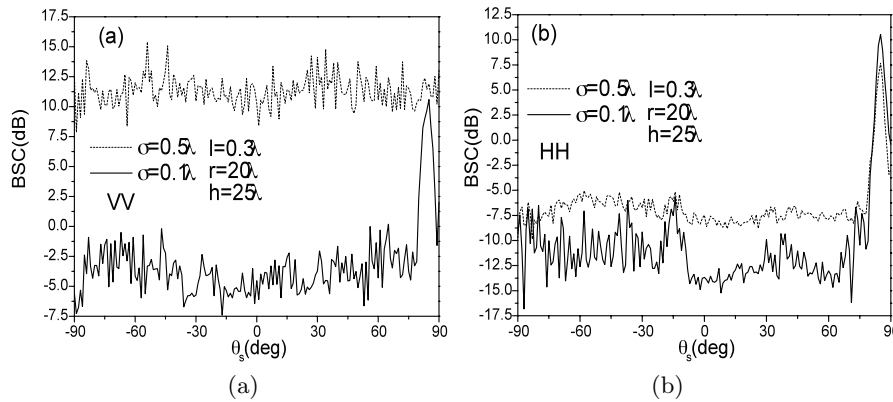
Figure 12. BSC for different σ and polarization.

from Gaussian surface only and surface coupling with target, the BSC
from the PEC Gaussian surface with/without a cylinder at incident
angle $\theta_i = 85°$ are presented in Fig. 10 for different parameters of
roughness. It is obviously that, the scattering pattern of coupling
model exhibits more oscillation for the whole scattering region than
that of the surface only (without target). Moreover, the scattering
coefficient for the composite model is larger than of the surface only in
the direction far from the specular direction.

In Fig. 11 and Fig. 12, the influences of rough surface parameters,
which includes the correlation length l, the root mean square height
σ, on the composite scattering for 2-D cylinder above 1-D large scale
PEC Gaussian rough surface at low grazing incident angle $\theta_i = 85°$

are analyzed by the parallel MOM on PC Clusters. By comparing the BSC in Fig. 11(a) and Fig. 11(b), it is easily found that, the BSC of VV polarization is visually larger than that of HH polarization in the non-specular direction. In Fig. 11, it can be concluded that the BSC near the specular direction with different correlation length l are nearly identical for the same σ, and with decreasing of l, the BSC far from the specualr direction increases for both HH and VV polarizations. The primary reason for this is due to the fact that for the smaller correlation length l, the height fluctuation of Gaussian rough surface becomes more heavily, which leads to a more incoherent scattering contribution to the BSC in non-specular direction. This phenomenon is similar as that of only surface scattering. Fig. 12 presents the dependence of the BSC on σ. As can be seen in Fig. 12, the influence of σ on the BSC at low grazing incident angle is significant. The BSC of non-specular direction increases with larger σ, especially for the VV case, this phenomenon mainly results from that the roughness of the Gaussian surface increases with increasing of σ, and in this case, the scattering of other direction (except for the specular direction) enhances with increasing the surface roughness.

Figure 13 and Fig. 14 show the dependences of the BSC on the radius of cylinder r, the altitude of cylinder h with low grazing incidence ($\theta_i = 85°$, HH polarization). It is seen that the BSC almost does not change with different r or h in the specular direction, while the BSC of the composite model increases with increasing r, especially for non-specular direction (shown in Fig. 13), this is mainly caused by the fact that the coupling scattered field increases as the coupling area between cylinder and surface becomes larger with the increase of r, which results in the total BSC of composite model increases. It is also found that the proportion of the coupling scattered field in the total scattered field becomes larger far from the specular direction and a larger oscillation of the total scattered field is observed with the varying of h (shown in Fig. 14). However, the BSC of the composite model decreases at a gentler rate with the increasing of h which means that the it is not sensitive to the large value of h.

5. CONCLUSIONS

By investigating the parallel MOM on PC Clusters, the EM scattering characteristics by a PEC cylinder above a large scale PEC Gaussian rough surfaces at low grazing incident angle is studied. The paper presented the detail procedure of the parallelized CGM according to the property of the MPI. The efficiency and validity of the parallel method are then discussed. Finally, the effects of rough surface
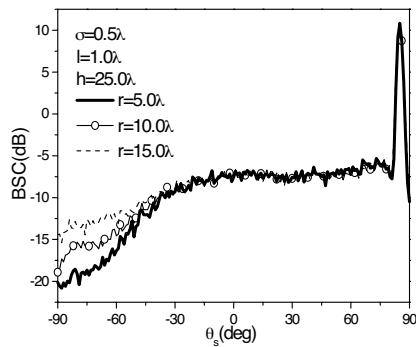
Figure 13. BSC for different radius of cylinder r.
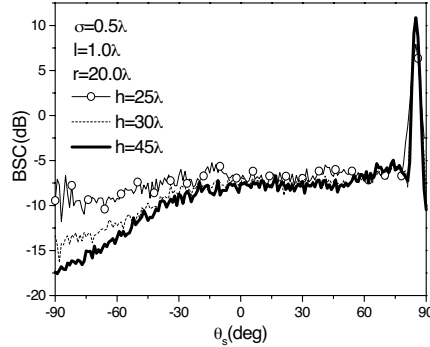
Figure 14. BSC for different altitude of cylinder h.

parameters, the radius and the altitude of cylinder, and polarization on the BSC at low grazing incident angle are analyzed. It is worth noting that the parallel MOM based on MPI through PC Clusters parallel computing system supplies a novel technique for solving 1-D large scale rough composite scattering problem. The further work is to develop this method to extend the study to three-dimensional problems, which are especially a grand challenge because the ordinary numerical methods may be intractable for electrically large composite surface geometries. Fast and advanced numerical methods combined with parallel methods must be exploited such as Fast Multipole Method (FMM) [23, 24] and Sparse Matrix Canonical Grid (SMCG) [25, 26]. The results of these investigations will appear in the future submissions.

ACKNOWLEDGMENT

REFERENCES

1. Guo, L. X. and Z. S. Wu, "Application of the extended boundary condition method to electromagnetic scattering from rough dielectric fractal sea surface," *Journal of Electromagnetic Waves and Applications*, Vol. 18, No. 9, 1219–1234, 2004.

2. Kizilay, A. and S. Makal, "A neural network solution for identification and classification of cylindrical targets above perfectly conducting flat surfaces," *Journal of Electromagnetic Waves and Applications*, Vol. 21, No. 14, 2147–2156, 2007.

3. Li, J., L. X. Guo, and H. Zeng, "FDTD investigation on bistatic scattering from a target above two-layered rough surfaces using UPML absorbing condition," *Progress In Electromagnetics Research*, PIER 88, 197–211, 2008.

4. Li, X. F., Y. J. Xie, and R. Yang, "High-frequency method analysison scattering from homogenous dielectric objects with electricallylarge size in half space," *Progress In Electromagnetics Research B*, Vol. 1, 177–188, 2008.

5. Li, J., L. X. Guo, and H. Zeng, "FDTD investigation on the electromagnetic scattering from a target above a randomly rough sea surface," *Waves in Random and Complex Media*, Vol. 18, No. 4, 641–650, 2008.

6. Chen, X. J. and X. W. Shi, "Backscattering of electrically large perfect conducting targets modeled by NURBS surfaces in half-space," *Progress In Electromagnetics Research*, PIER 77, 215–224, 2007.

7. Zhang, Y., Y. E. Yang, H. Braunisch, and J. A. Kong, "Electromagnetic wave interaction of conducting object with rough surface by hybrid SPM/MOM technique," *Progress In Electromagnetics Research*, PIER 22, 315–335, 1999.

8. Wang, X., C. F.Wang, Y. B. Gan, and L. W. Li, "Electromagnetic scattering from a circular target above or below rough surface," *Progress In Electromagnetics Research*, PIER 40, 207–227, 2003.

9. Chiu, T. and K. Sarabandi, "Electromagnetic scattering interaction between a dielectric cylinder and a slightly rough surface," *IEEE Trans. Ant. Propag.*, Vol. 47, No. 5, 902–913, 1999.

10. Harrington, R. F., *Filed Computation by Moment Method*, IEEE Press, New York, 1993.

11. Pino, M. R., L. Landesa, J. L. Rodriguez, F. Obelleiro, and R. J. Burkholder, "The generalized forward-backward method for analyzing the scattering from targets on ocean-like rough surfaces," *IEEE Trans. Antennas Propag.*, Vol. 47, No. 6, 961–969, 1999.

12. Li, Z. and Y.-Q. Jin, "Bistatic scattering from a fractal dynamic rough sea surface with a ship presence at low grazing angle incidence using the GFBM/SAA," *Microwave Opt. Technol Lett.*, Vol. 31, No. 2, 146–151, 2001.

13. Tsang, L., C. H. Chan, K. Pak, and H. Sangani, "Monte-Carlo simulations of large-scale problems of random rough surface scattering and applications to grazing incidence with the BMIA/canonical grid method," *IEEE Trans. Antennas Propag.*, Vol. 43, No. 8, 851–859, 1995.

14. Chan, C. H. and L. Tsang, "Monte-Carlo simulations of large-scale one-dimensional random rough surface scattering at near-grazing incidence: Penetrable case," *IEEE Trans. Antennas Propag.*, Vol. 46, No. 1, 142–149, 1998.

15. Li, Q., C. H. Chan, and L. Tsang, "Monte Carlo simulations of wave scattering from lossy dielectric random rough surfaces using the physics-based two-grid method and the canonical-grid method," *IEEE Trans. Antennas Propag.*, Vol. 47, No. 4, 752–763, 1999.

16. Johnson, J. T., "Numerical study of scattering from an object above a rough surface," *IEEE Trans. Antennas Propag.*, Vol. 50, No. 10, 1361–1367, 2002.

17. Hestenes, M. R. and E. Stiefel, "Method of conjugate gradients for solving linear systems," *J. Res. Natl. Bur. Stand.*, Vol. 49, 409–436, 1952.

18. Thorsos, E., "The validity of the Kirchhoff approximation for rough surface scattering using a Gaussian roughness spectrum," *J. Acoust Soc. Am.*, Vol. 83, No. 1, 78–92, 1988.

19. Tsang, L., J. A. Kong, K.-H. Ding, and C. O. Ao, *Scattering of Electromagnetic Waves: Numerical Simulations*, John Wiley & Sons, 2001.

20. Ye, H. and Y.-Q. Jin, "Parameterization of the tapered incident wave for numerical simulation of electromagnetic scattering from rough surface," *IEEE Trans. Antennas Propag.*, Vol. 53, No. 3, 1234–1237, 2005.

21. Message Passing Interface Forum, MPI: A message-passing interface standard, June 1995. http://www. mpi-forum.org/docs/mpi-11-html/mpi-report.html.

22. Lauria, M. and A. Chien, "MPI-FM: High performance MPI on workstation clusters," *Journal of Parallel and Distributed Computing*, Vol. 40, 4–18, 1997.

23. Rokhlin, V., "Rapid solution of integral equations of scattering theory in two dimensions," *J. Comput. Phys.*, Vol. 86, 414–439, 1990.

24. Lu, C. C. and W. C. Chew, "Fast algorithm for solving hybrid integral equations," *IEE Proceedings-H*, Vol. 140, 455–460, 1993.

25. Li, S. Q., C. H. Chan, and M. Y. Xia, "Multilevel expansion of the sparse-matrix canonical grid method for two-dimensional random rough surfaces," *IEEE Trans. Antennas Propag.*, Vol. 49, No. 11, 1579–1589, 2001.

26. Xia, M. Y., C. H. Chan, S. Q. Li, B. Zhang, and L. Tsang, "An efficient algorithm for electromagnetic scattering from rough surfaces using a single integral equation and multilevel sparse-matrix canonical-grid method," *IEEE Trans. Antennas Propag.*, Vol. 51, No. 6, 1142–1149, 2003.